HHS Public Access

Author manuscript

J Vis Exp. Author manuscript; available in PMC 2023 July 06.

Confocal and Super-Resolution Imaging of Polarized Intracellular Trafficking and Secretion of Basement Membrane Proteins during *Drosophila* Oogenesis

Hemin P. Shah[1], **Olivier Devergne**[1]

[1]Department of Biological Sciences, Northern Illinois University

Abstract

The basement membrane (BM) - a specialized sheet of extracellular matrix present at the basal side of epithelial cells - is critical for the establishment and maintenance of epithelial tissue morphology and organ morphogenesis. Moreover, the BM is essential for tissue modeling, serving as a signaling platform, and providing external forces to shape tissues and organs. Despite the many important roles that the BM plays during normal development and pathological conditions, the biological pathways controlling the intracellular trafficking of BM-containing vesicles and how basal secretion leads to the polarized deposition of BM proteins are poorly understood. The follicular epithelium of the *Drosophila* ovary is an excellent model system to study the basal deposition of BM membrane proteins, as it produces and secretes all major components of the BM. Confocal and super-resolution imaging combined with image processing in fixed tissues allows for the identification and characterization of cellular factors specifically involved in the intracellular trafficking and deposition of BM proteins. This article presents a detailed protocol for staining and imaging BM-containing vesicles and deposited BM using endogenously tagged proteins in the follicular epithelium of the *Drosophila* ovary. This protocol can be applied to address both qualitative and quantitative questions and it was developed to accommodate high-throughput screening, allowing for the rapid and efficient identification of factors involved in the polarized intracellular trafficking and secretion of vesicles during epithelial tissue development.

Introduction

The basement membrane (BM) is a thin sheet of layered cell-adherent extracellular matrix (ECM) critical for epithelial structure and morphogenesis[1]. It comprises ~50 proteins and is found ubiquitously underlying the epithelial and endothelial cells, and ensheathing skeletal, smooth, and heart muscle cells and adipocytes[1,2,3]. The three main components of the BM at the basal side of the epithelial cells are Collagen IV, Perlecan, and Laminins. The BM underlies the epithelial cells and is responsible for many functions, including tissue separation and barrier, growth and support, and cell polarization[2,3,4,5,6,7,8,9,10,11,12]. Its role as a signaling platform regulates the morphology and differentiation of epithelial cells

Corresponding Author: Olivier Devergne, odevergne@niu.edu.

A complete version of this article that includes the video component is available at http://dx.doi.org/10.3791/63778.

Disclosures

The authors have nothing to disclose.

and tissues during development[3,13,14]. Moreover, the mis-regulation of the BM and/or a breach in its integrity are the primary causes of many pathological conditions, including tumor metastasis[2,15,16]. Despite the essential functions performed by the BM during tissue and organ morphogenesis, the components of the biological pathway(s) dedicated to the polarized intracellular trafficking and secretion of BM proteins are vaguely known.

To study the intracellular trafficking of BM-containing vesicles and the secretion of BM proteins by epithelial cells, the follicular epithelium (FE) of the *Drosophila* ovary is a powerful model system (Figure 1). A *Drosophila* ovary comprises 16–20 long, tube-like structures, called ovarioles (Figure 1A,B)[17,18,19]. Each ovariole can be thought of as an egg assembly line, with the age progression of egg chambers (which each gives rise to an egg) that begins at the anterior end and moves posteriorly, until the mature egg exits through the oviduct. Each egg chamber is encapsulated by the FE, a monolayer of somatic follicle cells (FCs), that surrounds the central germline cells (GCs). The FE is highly polarized with a distinct apical-basal polarity where the apical domain faces the germline, and the BM proteins are secreted basally[18,19].The FCs actively secrete all of the major components of the BM, including Collagen IV, Perlecan, and Laminins[20,21]. In epithelial cells such as FCs, the BM components are produced and require a specialized polarized secretion pathway for their deposition extracellularly. For example, in the case of the most abundant component of the BM, Collagen IV (Coll IV), the details surrounding its polarized intracellular trafficking and secretion are vague despite its production and deposition being the focus of many studies. Coll IV is translated in the endoplasmic reticulum (ER), which is also where each fibril - composed of three polypeptides (two α1 chains and one α2 chain) - is assembled into a triple helix[22]. Proper Coll IV folding and function require ER chaperones and enzymes, including lysyl and prolylhydroxylases such as Plod and PH4αEFB[20,22,23,24,25,26]. These posttranslational enzymes regulate the ER sorting of Coll IV, as the loss of each causes Coll IV to be trapped in the basal ER[20,23,24,25,26]. Then, newly synthesized Coll IV exits the ER for the Golgi in COPII-coated vesicles. The cargo receptor Tango1 aids in packaging collagens into sizable Golgi-bound vesicles that can accommodate large multimeric proteins[20,27]. Once Coll IV is packaged into intracellular exocytic vesicles, it is specifically secreted basally from epithelial cells. To direct BM deposition to the basal side, epithelial cells require another set of factors specifically dedicated to polarized BM secretion. Using the FE of the *Drosophila* ovary, a few components of this novel cellular process have been characterized, including the nucleotide exchange factors (GEFs) Crag and Stratum, the GTPases Rab8 and Rab10, as well as the levels of the phosphoinositide PI(4,5)P2, and Kinesin 1 and 3 motor proteins[20,28,29,30,31]. These components are critical in ensuring the polarized distribution of BM proteins.

To monitor the intracellular localization of BM proteins in the FE, endogenously tagged basement membrane proteins (protein traps), such as Viking-GFP (Vkg-GFP or α2 Coll IV-GFP) and Perlecan-GFP (Pcan-GFP) can be used[32,33]. These protein trap lines have been shown to accurately reflect the endogenous distribution of BM proteins and allow for more sensitive detection of vesicular trafficking[28,30]. The components involved in the polarized deposition of BM in the FE were first characterized using protein trap lines for Vkg-GFP and Pcan-GFP[20,28,29,30]. Protein traps can be used in different genetic backgrounds, including mutants and *Gal4* lines[34]. Moreover, protein traps can be used in combination with

fluorescent dyes and/or fluorescence immunostaining, allowing for precise characterization of the localization of BM proteins when comparing wild-type and mutant conditions[35].

To accurately and efficiently assess the distribution and localization of BM protein-containing vesicles, confocal laser scanning microscopy (CLSM) and super-resolution imaging techniques present a significant advantage to other imaging approaches. These approaches couple high-resolution imaging with relative ease of use. CLSM is a microscopy technique that allows for an improved optical resolution by scanning the specimen with a laser in a raster scan manner using galvanometers. The pinhole aperture is a core component of a confocal microscope. By blocking the out-of-focus signals coming from above or below the focal plane, the pinhole aperture results in a highly superior resolution in the z-axis[36]. This also makes it possible to obtain a series of images in the z-plane, called a z-stack, corresponding to a series of optical sections. z-stacks subsequently create a 3D image of the specimen, *via* 3D reconstruction, with the aid of imaging software. Conventional epifluorescence (widefield) microscopes, unlike confocal microscopes, allow out-of-focus light to contribute to image quality, decreasing image resolution and contrast[36,37]. This makes epifluorescence microscopy a less attractive candidate when studying protein localization or colocalization.

Although CLSM is a suitable approach for various applications, including imaging and characterization of the intracellular trafficking of BM proteins, it still presents an issue when imaging samples below Abbe's diffraction limit of light (200–250 nm). When imaging such samples, confocal microscopy, especially when using an oil objective, can result in high resolution. However, super-resolution techniques surpass the limit of confocal microscopy. There are various approaches to achieve super-resolution microscopy, each with specific resolution limits, and each appropriate for different analyses. These approaches include photoactivated localization microscopy (PALM) or stochastic optical reconstruction microscopy (STORM), stimulated emission depletion microscopy (STED), structured illumination microscopy (SIM), and Airyscan (super-resolution) microscopy[38,39,40,41,42,43,44,45,46]. Although Airyscan has a coarser resolution than PALM/STORM, STED, and SIM, it can still achieve a resolution of up to ~120 nm (about twice the resolution of CLSM). Furthermore, this super-resolution microscopy approach has been shown to have an advantage over SIM and other super-resolution techniques when imaging thick samples and samples with a low signal-to-noise ratio[47,48].

Airyscan is a relatively new super-resolution confocal microscopy technology[46]. Unlike traditional CLSMs, which use the pinhole and single point detectors to reject out-of-focus light, this super-resolution approach uses a 32-channel gallium arsenide phosphide (GaAsP) photomultiplier tube area detector that collects all of the light at every scan position[45]. Each of the 32 detectors work as a small pinhole, reducing the pinhole size from the traditional 1.0 Airy Unit (A.U.) to an enhanced 0.2 A.U., enabling an even higher resolution and signal-to-noise ratio, while maintaining the efficiency of a 1.25 A.U. diameter[45]. Furthermore, the linear deconvolution used by Airyscan results in up to a 2x increase in resolution[45]. Taking this into consideration, CLSM, and specifically super-resolution microscopy, are well-suited to study BM proteins and proteins that regulate the basal deposition of BM proteins, as they can produce very high-resolution images for localization and colocalization studies,

thereby providing new insights in the spatial, temporal, and molecular events that control these processes.

An alternative approach to confocal microscopy that can be used to perform localization experiments is image deconvolution. Since widefield microscopy allows out-of-focus light to reach the detectors, mathematical and computational deconvolution algorithms can be applied to remove or reassign out-of-focus light from images obtained by widefield microscopy, thereby improving the resolution and contrast of the image[49]. Deconvolution algorithms can also be applied to confocal images to further increase resolution and contrast, producing final images almost comparable to that of super-resolution microscopy[50]. Airyscan makes use of Weiner filter-based deconvolution along with Sheppard's pixel reassignment, resulting in a highly improved spatial resolution and signal-to-noise ratio. Compared to confocal microscopy, an increase of 2x in resolution in all three spatial dimensions (120 nm in x and y, and 350 nm in z) is observed when using this super-resolution microscopy technique[45,51].

This manuscript provides detailed and optimized protocols to stain, acquire, and visualize the intracellular trafficking and deposition of BM proteins using the FE of the *Drosophila* ovary as a model system coupled with confocal and super-resolution microscopy. *Drosophila* lines expressing endogenously tagged basement membrane proteins, e.g., Vkg-GFP and Pcan-GFP, are efficient and accurate tools to visualize BM protein trafficking and secretion. In addition, they can be easily used in different genetic backgrounds, including mutant and *Gal4/UAS* lines[34]. Although endogenously tagged basement membrane proteins are recommended, the use of antibodies against specific BM proteins is also compatible with the described protocols. These protocols are particularly useful for scientists who are interested in studying intracellular trafficking and the secretion of BM proteins in intact epithelial tissue using confocal and super-resolution imaging. Moreover, the ability to combine epithelial tissue analysis with the expansive tools of *Drosophila* genetics makes this approach especially powerful. Finally, these protocols could be easily adapted to study vesicular trafficking and sorting of other proteins of interest.

Protocol

1. Fly preparation for ovary dissections

1. Put 10–15 *Drosophila melanogaster* female flies (1–2 days old) of the desired genotype in a narrow vial containing ~8 mL of *Drosophila* fly medium sprinkled with a small amount of granulated baker's yeast 2–3 days prior to dissection at 25 °C. Adding a few males to the vial can boost egg chamber yield. However, ensure that the total number of flies does not exceed 20 as this can negatively affect ovary development.

   NOTE: Description of *Drosophila* males and females, and useful tips and advice for scientists without prior *Drosophila* experience can be found in the cited articles[34,52]. Adding yeast will stimulate egg production and generate ovaries with different stages represented. Moreover, it will also fatten the ovaries and

make them easier to excise. Wet yeast can also be used instead of granulated yeast, however, for weaker stocks, the flies may get stuck and die.

2. Ovary dissection and fixation

NOTE: For additional resources on ovary dissection and staining, readers are directed to the cited protocols[53,54,55].

1. On the day of dissection, prepare fresh fixation solution with a final concentration of 4% paraformaldehyde (PFA) by diluting the PFA stock solution in 1x phosphate buffer saline (PBS).

2. Anesthetize the flies using CO_2 and place them on a fly pad. Keep the flies anesthetized until dissection. Consider flies properly anesthetized once their movements have ceased, which usually takes 10–20 s.

   NOTE: Although using CO_2 is recommended as a safer and faster option, flies can be anesthetized using ice.

3. Place a glass concave slide or staining dish with shallow depression wells under a dissecting microscope and fill the wells with 1x PBS.

4. Grasp a female fly at the lower thorax using a pair of forceps. Ensure the sex of the flies by the absence of male genitalia at the posterior end of the abdomen and the absence of sex combs on their forelegs as a secondary characteristic[52]. Dissect flies individually using another pair of forceps (step 2.5) while submerging them into wells filled with 1x PBS under the dissecting microscope (20x magnification is recommended).

5. While looking through the dissecting microscope, use another pair of forceps to tug at the posterior part of the fly abdomen, making the internal organs (e.g., ovaries, gut) visible.

6. Gently squeeze the anterior part of the fly abdomen (as with a tube of toothpaste) to force the ovaries out of the abdomen. This method should keep the ovaries intact. Detach and carefully remove other organs and fly debris.

7. Using forceps or dissecting needles, separate the ovarioles of the ovary while keeping the overall ovary structure intact. The purpose of this step is to break the muscle sheath covering the ovaries and allow for a more efficient and homogenous staining.

8. Quickly transfer the ovaries to a 1.5 mL microcentrifuge tube containing 1x PBS and keep the tube on ice until all the flies are dissected. Do not keep the tube on ice if microtubules or microfilaments (or vesicles trafficked by these cytoskeletal components) are to be visualized as this can cause depolymerization.

9. Once all the ovaries are dissected and transferred to a microcentrifuge tube, allow them to sink to the bottom of the tube and remove all but ~50 μL of the PBS. Add 1 mL of 4% PFA and place on a nutating platform rocker for 15 min. Importantly, check whether the ovaries are moving back and forth in the fixation

solution to allow for proper fixation as incomplete fixation could lead to staining and imaging issues.

NOTE: The speed of the nutator is not crucial. While some nutators have a speed control, others come with a preset speed. The preset speed is sufficient, and if adjustable, set to 40–50 rpm.

10. Remove the fixation solution (as in step 2.9), and then perform two quick washes with 1 mL of 1x PBS containing 0.1% Triton-X 100 (1x PBST), by gently inverting the microfuge tubes 5–6 times. Then, proceed with four 10–15 min washes (long wash) with 1 mL of 1x PBST (40–60 min total).

    NOTE: It is recommended to use 1x PBS + 0.1% Triton-X 100 for washes as increasing the percentage of detergent could result in GFP denaturation, leading to decreased fluorescence and detection of GFP-tagged BM proteins.

11. For dye staining, e.g., DNA and F-actin staining, proceed to step 3. For immunostaining, proceed to step 4. The ovaries can be stored in 1x PBST at 4 °C for up to 24 h before proceeding.

3. Standard DNA/F-Actin staining

1. After fixation and washing, remove PBST. Add 500 μL of DNA and F-Actin staining solution. To prepare the DNA/F-Actin solution, mix Hoechst (DNA stain; 1:1000 dilution of 1 mg/mL stock solution) and fluorophore-tagged phalloidin (F-actin stain; 1:500 dilution for Alexa Fluor 546 or 1:100 dilution for Alexa Fluor 647, each of 66 μM stock solution) in 500 μL of PBST.

2. Cover the tubes with aluminum foil to keep the ovaries and dyes in the dark to maintain the fluorescence for efficient imaging and incubate on a nutating platform rocker for 15 min.

3. After incubation, remove the DNA/F-Actin solution (as in step 2.9). Perform two quick washes and three long (10–15 min) washes in 1x PBST as described in step 2.10. Proceed to mounting as described in step 5.

4. Fluorescence immunostaining

NOTE: This is a standard immunostaining protocol for fluorescent imaging and is compatible with most primary antibodies.

1. Blocking and primary antibody immunostaining (Day 1)

    1. After fixation and washing, remove PBST as described in step 2.9. Add 1 mL of blocking solution (PBS + 5% BSA) and block the ovaries on a nutating platform rocker for 1 h minimum.

        NOTE: In addition to BSA, fetal bovine serum (FBS) or normal goat serum (NGS) can be added to the blocking solution. Alternatively, the ovaries can be blocked overnight on a nutating platform rocker at 4 °C.

2. Remove blocking solution as in step 2.9 and add 300 μL of primary antibody solution containing primary antibodies diluted at their appropriate concentrations (specific to the antibody used) in the blocking solution. Incubate overnight on a nutating platform rocker at 4 °C. The next day, remove the primary antibody solution and proceed to secondary antibody immunostaining.

   NOTE: Some primary antibodies can be saved and reused. In some instances, reused primary antibodies can reduce background staining, resulting in better imaging. However, reuse should be tested for each antibody to ensure efficiency.

2. Secondary antibody immunostaining (Day 2)

   1. After removing the primary antibody solution, perform two quick washes and four long (10–15 min) washes as in step 2.10. Carefully done repetitive washes using fresh 1x PBST will decrease non-specific background and lead to optimal imaging.

   2. Remove PBST as in step 2.9 and add 500 μL of secondary antibody solution containing fluorescent secondary antibodies that will detect the primary antibodies used. Protect the tube from light by covering it in aluminum foil from this point on for optimal conservation of fluorescence, which is critical for image acquisition and analysis.

      NOTE: The secondary antibody solution should contain secondary antibodies conjugated with fluorophores that do not overlap with endogenously tagged proteins. For example, if using GFP-tagged proteins, the use of Alexa Fluor secondary antibodies at red or far-red wavelengths is recommended (e.g., 546, 568, or 647 nm). Fluorescent dyes, such as Hoechst and Alexa Fluor 546 or 647 conjugated phalloidin, can be added to the secondary solution. These stains could be helpful to mark the overall cell structure (i.e., nuclei and F-Actin). Refer to step 3.1 for the concentrations.

   3. Incubate the ovaries in the secondary antibody solution on a nutating platform rocker for 2 h at room temperature. Perform two quick washes and four long (10–15 min) washes in 1x PBST as in step 2.10. Proceed to mounting as in step 5.

5. Mounting of stained ovaries

NOTE: This method works very well if the ovaries are well-developed and abundant. Careful mounting of the ovaries on the slide is critical for optimal imaging.

1. After the last wash, use a p1000 pipette to gently pipet the ovaries up and down in the tube to separate the egg chambers. Allow the egg chambers to sink to the bottom by keeping the tube in an upright position for 5–10 min. Careful separation of individual egg chambers is critical to achieve optimal image acquisition.

2. Remove PBST using a Pasteur pipet, leaving ~50 μL. Remove as much of the remaining PBST as possible using a p200 pipette. Add two drops of mounting medium, enough to spread evenly on a 22 mm x 22 mm coverslip. Ovaries can be stored in mounting medium in microcentrifuge tubes at 4 °C for up to 1 month prior to mounting.

   NOTE: Several different mounting media are available commercially; using hard-setting mountants, such as Aqua-Poly/Mount or ProLong Glass Antifade Mountant, is recommended to achieve optimal imaging conditions. The use of glycerol as a mounting medium is discouraged since it can lead to poor imaging conditions (e.g., fluorophore instability). For mounting media that do not polymerize, seal the coverslip using a coverslip sealant/ nail polish to secure it in place.

3. Label a glass slide and wipe it with soft, dust free paper to remove dust and fingerprints. Cut off the end of a p200 pipette tip to allow easy transfer of the viscous mounting medium to the slide from the microcentrifuge tube. Next, slowly transfer all the egg chambers in the mounting medium to the glass slide, ensuring not to create bubbles.

4. Under a dissecting microscope, gently spread out the mounting medium and separated egg chambers using a new p200 tip or forceps to cover an area approximately the size of the coverslip.

5. Using forceps, carefully place the coverslip (cleaned with dust-free paper) on the egg chambers at an angle to avoid bubbles.

6. Store the slide at room temperature on a flat surface in the dark for 2 days to polymerize. Once the mounting media has cured, the slide can be stored at 4 °C in the dark for a few weeks for imaging.

   NOTE: It is important for hard setting mounting medium to polymerize before imaging. If the medium has not yet polymerized, the ovaries will float under the coverslip, affecting image acquisition. Moreover, the optimal reflective index of mounting media is only achieved after it completely sets (see the manufacturer's information for details).

7. Alternative mounting method: This method is recommended to reduce tissue loss if ovaries are not abundant. In this method (described below), separate the ovarioles and the egg chambers on the slide while mounting, instead of separating them in a microcentrifuge tube by pipetting as described in step 5.1.

   1. After the last wash, remove all but ~100 μL of the wash solution. Using a Pasteur pipette or p1000 pipette, transfer the intact ovaries in PBS to the slide. Using a p200 pipette, carefully remove as much PBST from the slide as possible. Use a dust-free paper to wipe away the PBST, if needed. Do not touch the ovaries.

   2. Add two drops of mounting media. Carefully separate the ovarioles and egg chambers using forceps or dissecting needles. Remove and discard

extraneous tissue, and then spread out the egg chambers and ovarioles in the mounting medium. Proceed to steps 5.5–5.6.

6. Confocal image acquisition

NOTE: This section provides key parameters to achieve optimal image acquisition using any confocal microscope (Figure 2).

1. Set up the microscope and locate the sample as described below.
    1. Before imaging, it is crucial to locate the region of interest (ROI) using the eyepiece of the fluorescence microscope. Use a low magnification objective (20x) or the objective to be used for image acquisition (i.e., 40x or 63x). Select an egg chamber to image.

        NOTE: For image acquisition, using high magnification objectives such as 40x or 63x is recommended (see 6.2.1).
    2. Once the ROI is selected, proceed to image acquisition; proceed to step 6.2 for confocal imaging, and step 7 for super-resolution imaging.
2. Select the key parameters for optimal image acquisition as described below (examples of key parameters for the representative images are given in Table 1).
    1. Selecting an objective: For confocal image acquisition of the intracellular trafficking and secretion of BM proteins in the FE, use a 40x or 63x objective.

        NOTE: To achieve the best resolution possible, the use of Plan-Apochromat objectives, with high numerical aperture (NA) that provide the highest achromatic correction, is highly recommended.
    2. Selecting lasers for each channel/track: For GFP, use laser 488 nm; for DAPI or Hoechst, use laser 405 nm; for Alexa Fluor 546 or 568, use laser 561 nm; and for Alexa Fluor 647, use laser 640 nm.

        NOTE: Each laser selection will result in a different channel/track formation. Here, the term channel refers to the image formed by the recorded intensity distribution for excited fluorophores for the selected ROI at the specific wavelength of each channel.
    3. Pinhole setting: To reduce out-of-focus light during image acquisition, set the pinhole for each channel to 1 AU.
    4. Laser intensity and detector gain settings: To fine tune the image sensitivity, use both the detector master gain and laser power. To properly set the image sensitivity, a range indicator is recommended. Set both the master gain and laser power to have a proper sensitivity where the structures of interest (e.g., BM-containing vesicles) are clearly visible while avoiding detector saturation.

        NOTE: To avoid photobleaching, use the minimal laser power necessary. It is recommended to increase the detector gain first while

using the lowest laser power possible. If an increase of the detector gain cannot achieve the desired intensity, then increase the laser power. Laser power intensity between 0.5%−1.2% is recommended.

5. Frame size: it is recommended to use the optimal image size determined by the acquisition software. For most applications, use a maximal resolution of 1024 × 1024. Higher resolution will significantly increase the acquisition time.

6. Scan speed: Use a scan speed between 6–9, which is safe for most samples. If the sample is noisy, use a slower scan speed to improve signal-to-noise ratios. However, low scan speeds increase photobleaching and acquisition time.

7. Mean intensity averaging: To improve image quality, use mean intensity averaging *via* successive scans with identical settings. For most cases, use an averaging of two to improve signal-to-noise ratios without photobleaching the sample.

8. Zoom: Adjust the scan area using the zoom function. Use a zoom between 2x-4x with both 40x and 63x objectives as the most effective value to clearly visualize BM-containing vesicles in the FE. Carefully select the minimal ROI to reduce the acquisition time.

3. To acquire a z-stack using Zeiss Zen software, use the following Z-sectioning parameters and set them as described below.

   NOTE: Vesicles and other intracellular structures containing BM proteins are 3-dimensional (3D) structures. Acquiring a z-stack through the FE will significantly improve image quality and resolution. Usually, a range spanning the thickness/depth of the tissue is sufficient to efficiently visualize intracellular localization. For optimal 3D reconstruction, using the optimal interval that is determined by the software is recommended. For 40x and 63x objectives, avoid intervals higher than 0.5 μm between each z-section to allow for optimal 3D reconstruction.

   1. Click on the **z-Stack** checkbox in the main area under the **Acquisition** tab. Select the **All Tracks Per Slice** scanning mode for the z-stack. This will result in a change in channel tracks for each z-position slice.

   2. Select the desired channel to observe the specimen and click on **Live** to start a live scan. Use of the channel needed to detect the GFP-tagged BM protein is recommended.

   3. Set a range for the z-stack as described. Using the fine adjustment knob on the microscope, find the z-location for one end of the specimen, and click on **Set First**. Similarly, find the z-location for the other end of the specimen and click on **Set Last**.

4. For each location in the z-stack, click on each channel separately with the range indicator selected, and adjust the intensity of the laser and the master gain as needed, as described in step 6.2.4.

5. Set the interval for the z-stack to assign the step size as recommended in the NOTE below step 6.3. Click on **Start Experiment** to begin z-stack acquisition.

7. Super-resolution image acquisition

1. Select an Airyscan compatible objective. To visualize the intracellular localization of BM protein, use of a 63x oil objective is optimal (Figure 3). Set the objective to 63x and gently place a drop of immersion oil on its lens. Position the slide on the objective with coverslip facing the objective to locate the specimen.

2. Select a configuration with appropriate settings for the fluorophore to image as described below.

    1. Click on the **Smart Setup** button in the **Acquisition** tab to configure a new experiment. Select **Airyscan** (super-resolution); when this is selected, a further selection between Resolution (Airyscan SR), SNR/ sensitivity (Airyscan Confocal), and Speed (Multiplex SR-2Y) will be required. For fixed tissue, select **Resolution** as that will result in the best acquisition.

    2. Click on **+** in the **Configure Your Experiment** box to add tracks/ channels. Select the tracks for specific dyes from the Dye Database. For a multi-channel experiment, add each track as needed by selecting the appropriate dyes.

    3. After all the tracks have been added, select one of the experiment proposals provided by the software. For this experiment, use **Best Signal**, as although the speed will be a little slower compared to the Smartest (Line) proposal, it will create the best hardware settings for each dye, resulting in maximum signal gain and minimal emission crosstalk. Once the experiment has been set and loaded, it will appear in the Imaging Setup window in the Acquisition tab.

    4. Once a smart setup is selected, the range of wavelengths for the detector GaAsP-PMT will automatically be selected. Adjust the range by moving the scroll bar at the bottom to increase or decrease the range or completely move the range to another region as required. Use this to make sure that the ranges of two different channels do not overlap to avoid crosstalk. Save the configuration to reuse in the future.

3. Once the configuration is set, proceed to adjust the zoom and scan area as in step 6.2.8. Optimize the scan area to focus on the region of interest to reduce scan time and storage space. Proceed to acquiring images.

4. For each individual channel, select a track under **Channel** and click on **Live**. Adjust the master gain and laser power using the range indicator tool as described in step 6.2.4 and follow all the guidelines described to avoid saturated pixels. Confirm that the hexagonal detector view is centered and aligned by clicking on the **Airyscan Detector View** button. In most cases, the hexagonal detector view is automatically centered and aligned. Repeat for additional channels.

5. In the Acquisition mode toggle window, under **Image Size**, click on **SR** (super-resolution-limited pixel count) to maximize the capabilities of the detector. This will adjust the frame size automatically.

6. Keep the averaging to **None** as it is usually not necessary, and this will decrease the scan time. In some cases, an averaging of 2x may improve the signal-to-noise ratio.

7. Collect raw data with 8-bit data depths. Click on **Snap** to acquire an image. To acquire a z-stack, follow step 6.3.

8. Perform image processing as described below. This will produce a 16-bit image.

    1. Once the image or z-stack is obtained, click on the **Processing > Method** and select **Airyscan Processing**.

    2. Perform auto filter to start with and perform further manual processing by changing the SR value to obtain the best results for the sample. Once the optimal SR value has been determined, click on **Apply** to generate a processed image. In the case of z-stack images, process either as one z-slice (Current Image [2D]) or as the whole z-stack by clicking on the **3D Processing** box.

8. Image processing and data analysis (orthogonal projection, 3D reconstruction and intensity profile)

NOTE: For this method, the steps used to generate orthogonal projections, 3D reconstructions, and intensity profiles are described for the Zen software (see Table of Materials). Similar data analyses may also be performed with ImageJ software[56].

1. Perform orthogonal projection as described below (Figure 4).

    1. Once a z-stack has been obtained using confocal or super-resolution microscopy, generate an orthogonal projection to view the vesicles in the z-axis of the cell in a 2D view (compared to 3D reconstruction). To do this, click on the **Processing > Method** and select **Orthogonal Projection**.

    2. Under parameters, select the projection plane required. For a projection of the z-axis (z-stack), select the **Frontal (XY)** plane. Under **Method**, select **Maximum** to result in the highest quality projection.

3. Next, determine the thickness of the projection by selecting the starting position (starting z-slice), and determine the thickness (total number of z-slices) in the projection. It is ideal to select the thickness equal to that of one cell in the z-axis.

4. Once the parameters have been set, click on **Apply** to create the projection of the z-stack in an XY plane manner.

   NOTE: When creating orthogonal projections of multiple z-stacks to compare the amount of a particular object of interest, it is imperative to keep the thickness of the projection the same (or as close as possible) for data accuracy.

2. Perform 3D reconstruction as described below (Figure 5).

   1. Create 3D reconstructions of z-stacks to observe the localization and shape of structures. Do this for z-stacks acquired using confocal and super-resolution approaches. Process super-resolution z-stacks first using 3D processing as in step 7.8 for 3D reconstruction.

   2. To generate a 3D image, click on the **3D** icon in the preview window. Once clicked, a 3D tab will appear in the display control section in the bottom half of the screen. 3D views, such as Transparency, Volume, Maximum, Surface, and Mixed will be visible. Use Surface or Mixed views when viewing the structure of vesicles (preferable).

   3. For the highest quality image, select the **Precise** setting, as the fastest setting will be less accurate and lead to poor 3D rendering.

   4. Once the image has been generated, manipulate it by rotating and zooming to focus on a preferred location to view the objects of interest. Manipulate the 3D image under the **Appearance** tab.

   5. Once a satisfactory view has been obtained, under the 3D tab, select **Displayed Resolution**, and then click on **Create Image**. This will create a snapshot of the image in the same orientation as it was viewed and can be saved and exported in various file formats.

3. Generate an intensity profile as described below (Figure 7).

   NOTE: The distribution and intensity profiles of the pixels associated with the different fluorescent signals can be viewed as an overlay image to determine their colocalization.

   1. Once an optimal image has been acquired *via* confocal or super-resolution imaging, in the **View** panel of the **Preview** window, click on **Profile**. In the preview window, a histogram displaying the intensity profile as a function of distance will appear, as well as a table showing distances and intensity values.

   2. In the display controls area at the bottom of the screen, click on the **Arrow Tool** in the **Profile Definition** tab. Draw an arrow along the

length of the object for which the intensity profile of the different pixels needs to be assessed. To draw the arrow, zoom in on the image.

3. The intensity profile will appear on the left of the image preview, where the distance and the corresponding peaks along the path of the arrow will be displayed. To remove the histogram displayed on the image itself, uncheck the **Show Profile in Graphics** box.

4. In the **Dimensions** tab in the display control area, deselect any channels that are not to be included in the intensity profile.

5. In the **Graphics** tab, double-click on **Profile** shown under the **Annotations/Measurements** box to open the **Format Graphical Elements** pop-up box. Use this to change the color of the arrow as well as its style and stroke thickness. Close the box after selecting the desired settings.

6. Click on the **Profile View** tab. In the new image section, click on **Current View** and then on **Save As** to save the file. It is recommended to save the file as a .tif file to avoid data compression and loss.

Representative Results

The methods described herein can be used to efficiently and accurately image and characterize the intracellular trafficking and secretion of BM proteins in polarized epithelial cells, such as the FE of the *Drosophila* ovary. Next, we provide anticipated results obtained using the described methods, as well as helpful advice and potential pitfalls. To do so, Vkg-GFP, an endogenously tagged Vkg (*Drosophila* Col IV) is used. However, the same results can be achieved with other endogenously tagged BM proteins such as Pcan-GFP.

Setting optimal acquisition parameters (Figure 2)

To accurately characterize the intracellular trafficking and secretion of BM proteins, such as Vkg and Pcan, in epithelial cells, it is critical to properly set the acquisition parameters of the confocal microscope as described in the provided methods.

Using confocal microscopy, the intracellular localization of Vkg-GFP can be detected before being secreted and deposited basally in the FE (Figure 2A). It has been shown that after translation in the ER, Coll IV is transported to the Golgi before being packaged into intracellular exocytic vesicles. Using this imaging approach, we observe that Vkg-GFP accumulates in intracellular compartments with different shapes, potentially representing different organelles, endosomal compartments, and vesicle types (Figure 2A, arrows). In exocytic vesicles, Coll IV is already assembled into fibrils composed of three polypeptides: two α1 chains and one α2 chain (Vkg in *Drosophila*), leading to the formation of stretched vesicles that can also be visualized using confocal imaging (Figure 2A, arrows). Then, Coll IV is specifically secreted basally from epithelial cells where it is deposited in the BM (Figure 2, arrowheads).

If the acquisition parameters are not set properly, it is not possible to precisely observe the different morphologies and positions during the intracellular trafficking of BM proteins (Figure 2B,C). For example, if the acquisition parameters are optimized to visualize the extracellular BM and not intracellular structures, the BM protein-containing endosomal compartments and vesicles (here marked by Vkg-GFP) appear dim or are not visible (Figure 2B). Conversely, if the detectors are overly saturated, the intracellular localization of Vkg-GFP can be detected as in the optimal condition (compare Figure 2A and Figure 2C), but an increase in background fluorescence noise makes interpretation of the BM protein localization more difficult, particularly for colocalization experiments (see Figure 7). Overall, these data illustrate the importance of proper acquisition parameters to achieve accurate localization of BM proteins in the epithelium.

Setting optimal super-resolution and deconvolution parameters (Figure 3)

As illustrated for confocal image acquisition, it is also critical to properly set the acquisition parameters when using super-resolution microscopy to avoid under- or over-saturation. This super-resolution imaging approach also involves the careful configuration of deconvolution parameters to achieve super-resolution imaging (Figure 3). When deconvolution processing is optimally configured, super-resolution imaging significantly increases the resolution of intracellular structures containing BM proteins (Figure 3A, arrows), such as vesicles or Golgi structures (Figure 3A and Figure 7C), the BM itself (Figure 3A, arrowheads), and enhances the signal-to-noise ratio45. Super-resolution microscopy leads to a ~2x increase in resolution in all three spatial dimensions compared to confocal microscopy. This increase in resolution is clearly illustrated by the better-defined images of the intracellular trafficking of BM proteins and the BM taken using super-resolution imaging compared to those taken with standard CSLM (compare Figure 2A and Figure 3A).

If deconvolution parameters are not set properly, super-resolution is not optimally achieved, and the increase in resolution is lost. Under-processing of super-resolution images lead to blurred images, resulting in the intracellular localization of BM proteins appearing dim and not as well-defined as under optimal conditions (compare Figure 3B with Figure 3A). Conversely, over-processing of the images leads to grainy images, where the intracellular localization of BM proteins appears pixelated (Figure 3C). These data highlight the importance of using proper deconvolution parameters to achieve meaningful and representative images that reflect the intracellular distribution of BM proteins.

Altogether, these data clearly show and highlight the improved resolution of intracellular trafficking of BM proteins using super-resolution image processing compared to confocal microscopy. Specifically, this approach allows for better visualization of the intracellular trafficking of BM proteins by enhancing the resolution of the intracellular structures involved. This allows the comparison of different sizes and shapes of structures to better identify and characterize new factors involved in the polarized deposition of BM proteins in the FE.

Orthogonal projection and 3D reconstruction of optical z-sections (z-stack) through the FE to enhance visualization of the intracellular distribution of BM proteins (Figure 4 and Figure 5)

Since the intracellular distribution of BM proteins is present throughout the FE in 3D (x-, y-, and z-axes), orthogonal projection and/or 3D reconstruction of optical z-sections through the FE, using either super-resolution or confocal microscopy, can be used to assess the localization and the distribution of BM proteins inside wild-type or mutant cells (e.g., in Figure 4 and Figure 5).

Orthogonal projection allows for all of the z-sections acquired to be projected in a single plane. This method is particularly useful to show the overall distribution of vesicles and compartments containing BM proteins in a single image using confocal (Figure 4A) or super-resolution (Figure 4B) imaging. However, a significantly better resolution and lesser background noise result when using super-resolution microscopy than confocal microscopy (compare Figure 4B and Figure 4A).

Another approach to visualize the overall distribution of BM-containing compartments and vesicles is to generate a 3D reconstruction by assembling a stack of optical z-sections taken by confocal (Figure 5A) or super-resolution (Figure 5B) imaging. This approach can also be very efficient to assess the localization and distribution of intracellular BM proteins and the shape of compartments and vesicles containing Vkg-GFP, particularly when using super-resolution microscopy (Figure 5). Traditional confocal microscopy (Figure 5A) results in higher background noise when compared to super-resolution (Figure 5B), which when being accounted for in 3D rendering may result in artifacts. Furthermore, the lower resolution of confocal also results in the images created being less smooth and defined than those generated by super-resolution (compare Figure 5A and Figure 5B).

Characterization of the phenotypes associated with the loss of components involved in the polarized secretion of BM proteins using super-resolution imaging (Figure 6)

As shown thus far (Figure 2, Figure 3, Figure 4, and Figure 5), super-resolution microscopy and image processing can be used to assess the intracellular localization and distribution of BM proteins in the wildtype FE of the *Drosophila* ovary. Furthermore, this approach can also be used to determine and compare the localization of BM proteins in mutant or knockdown conditions. This, thereby, is an efficient method to characterize the role(s) of newly identified components dedicated to the polarized intracellular trafficking, secretion, and deposition of BM proteins.

The GTPase exchange factor (GEF) Crag has been shown to be a key component in a biological pathway dedicated to the polarized deposition of BM proteins[28]. In *Crag* knockdown FCs, BM proteins accumulate both apically and basally, indicating that Crag controls the polarized secretion of BM proteins such as Vkg-GFP (Figure 6). The use of super-resolution microscopy allows for better characterization of the phenotype resulting from the loss of Crag. For example, a strong apical accumulation of BM proteins, as well as the organization of the ectopic apical BM, is observed in *Crag*-knockdown FCs (Figure 6B, arrowheads). Moreover, when the phenotype is less aberrant, BM membrane accumulating

apically in small patches in FCs is detected (Figure 6B, arrows). Altogether, these data illustrate that super-resolution microscopy can be used to characterize mutant phenotypes to better understand the roles of components involved in the polarized deposition of BM.

Colocalization experiment using antibodies and endogenously tagged BM proteins imaged using confocal and super-resolution microscopy (Figure 7)

Finally, the use of antibodies against specific intracellular markers or newly identified components combined with endogenously tagged BM proteins can be used to better characterize the intracellular trafficking and secretion of BM proteins in the polarized epithelium. GM-130, a cis-Golgi marker, is used to illustrate this point. Before being packaged in secretion vesicles, Coll IV is transported to the Golgi. When the subcellular distribution of Vkg-GFP is assessed using confocal (Figure 7A,B) or super-resolution (Figure 7C,D) imaging, both approaches show that Vkg-GFP partially colocalizes with GM-130, confirming that Coll IV is sorted to the Golgi before secretion. However, an increase in the signal-to-noise ratio and a better resolution of the colocalization between Vkg-GFP and GM130 is observed when using super-resolution imaging (compare Figure 7A with Figure 7C).

Moreover, when the spatial distribution and levels of green (Vkg-GFP) and red (GM-130) pixels is quantified by measuring the fluorescence intensity of an optical section through FCs taken with confocal (Figure 7B) and super-resolution (Figure 7D) microscopy, the colocalization of Vkg-GFP and GM-130 is observed. The distribution of Vkg-GFP and GM-130 pixels is plotted in histograms in which overlaps of the Vkg-GFP and GM-130 peaks indicate their colocalization (Figure 7B’,D’). Thus, using this image analysis tool, the location of Vkg-GFP in specific intracellular compartments can be precisely determined. However, the comparison of histograms generated from confocal images (Figure 7B’) with super-resolution (Figure 7D’) images confirms that super-resolution microscopy produces better results, as can be seen by the higher intensity of peaks and reduced background noise represented by the lack of smaller peaks (compare Figure 7B’ and Figure 7D’) associated with super-resolution-generated histograms. Altogether, these data highlight that although confocal microscopy can be used to quantify colocalization, super-resolution is a more powerful approach, leading to a more efficient and precise quantification of the localization.

Discussion

The BM is critical for embryonic and organ morphogenesis, and adult physiological functions. Moreover, the BM acts as a signaling platform for the establishment and maintenance of epithelial polarity and provides tissues with support[2]. Yet, the mechanisms that regulate the proper placement of BM proteins are poorly understood. A better understanding of the biological pathways dedicated to the intracellular trafficking and polarized secretion of BM proteins requires a careful analysis of the components of these pathways and their roles in BM processing. One way to achieve this is to use confocal and super-resolution imaging. Here, we described methods for the preparation and staining or immunostaining of *Drosophila* ovaries to efficiently image the intracellular trafficking and secretion of BM proteins in the FE using confocal and super-resolution microscopy.

Advantages of protein trap and endogenously tagged proteins to visualize the intracellular trafficking and secretion of BM proteins in wild-type and mutant conditions

The provided protocol takes full advantage of protein traps and endogenously tagged BM proteins (e.g., Vkg-GFP and Pcan-GFP) to image and assess the localization and distribution of BM proteins in the FE in wild-type (control) and mutant conditions. These lines have important advantages over the use of antibodies against BM proteins. First, antibodies against specific proteins of interest are often rare and in low abundance. In addition, there are often issues with tissue penetrance associated with antibodies which can lead to inaccurate observation and assessment of the protein of interest. Moreover, protein trap lines can be inserted into different genetics background used to determine the functions of factors required for the proper deposition of the BM such as (i) methods to manipulate gene expression (e.g., UAS/Gal4), (ii) mutants, and (iii) RNA interference (RNAi) lines. Finally, these protein traps can be used to visualize the localization and function of BM using live imaging[57].

However, the fusion of a fluorescent tag to a protein of interest can interfere with its localization and functions. Thus, it is critical to evaluate any aberrant effects of the tag on the protein. One way to ensure that the addition of a fluorescent tag does not interfere with the function and localization of BM proteins is to determine whether the transgenic *Drosophila* line is homozygous viable. Both the Vkg-GFP and Pcan-GFP lines that are used in the different experiments described here and previously, are homozygous viable, indicating that the addition of a GFP tag does not interfere with the function of these essential proteins[29,30].

Importance of tissue preparation, fixation and staining for imaging

To efficiently and accurately image the FE, it is critical to prepare, fix, and stain the ovarian tissue properly as directed in this method. First, after dissection, carefully remove all other organs and fly debris before fixation. Using paraformaldehyde (PFA) to fix tissue is recommended, since it leads to bright GFP fluorescence and is compatible with most antibodies. However, PFA may not be compatible with all antibodies; some may require glutaraldehyde or methanol fixation. Moreover, to avoid background fluorescence due to non-specific binding of the primary antibody, the ovarian tissue should be incubated on a nutating platform rocker for at least 1 h in blocking solution, and extensively washed several times after primary and secondary antibody incubation as described in the protocol. Finally, proper mounting of the ovarian tissue is essential to achieve optimal imaging. This requires careful separation of individual egg chambers to avoid their stacking on top of each other. It is also important to let the mounting medium fully polymerize before imaging to avoid floating of the tissue under the coverslip. This further allows the mounting media to reach its optimal reflective index, which is very important for super-resolution imaging. Failing to do so will affect the image quality. Furthermore, the prepared slides can be stored for up to 1 month at 4 °C, before the fluorescence is quenched. In addition to the provided protocol, several other protocols are available for ovarian dissection and staining[53,54,55].

The use of proper acquisition and processing parameters is critical for optimal imaging and to assess the localization of BM proteins using confocal and super-resolution imaging

As described previously, it is critical to properly set the acquisition parameters for confocal and super-resolution imaging to obtain optimal images of the specimen. For image acquisition, the ROI must be carefully selected using the zoom function, and then setting the frame size and acquisition speed optimally. Moreover, as illustrated in Figure 2, it is critical to adjust the laser power and the detector gain appropriately to visualize intracellular trafficking without saturating the detectors. These parameters must be set very carefully to avoid underexposed or overexposed images (Figure 2). Underexposed images will result in low resolution images, in which the intracellular structures will be difficult to visualize and characterize (Figure 2B). Overexposed images due to the saturation of the detector lead to data misinterpretation, and colocalization artifacts (Figure 2C). If the aim is to determine the vesicular localization of endogenously tagged BM proteins, the fluorescence from GFP-tagged proteins (e.g., Vkg-GFP and Pcan-GFP) in the basal BM quickly saturates the detector. However, vesicles containing less GFP-tagged BM proteins will appear dim. Hence, it is important to set the image sensitivity using the BM-containing intracellular structures (e.g., vesicles), and not on the BM (Figure 2). Selecting pinhole size is also very important. Ideally, a pinhole size of 1 AU for each channel should be selected for best quality images, especially when the resolution in the z-axis is important. The smaller pinhole size is optimal for thinner optical sections. However, when optimal z-axis resolution is not required or a z-stack is not being captured, the pinhole size can be increased to avoid photobleaching. Furthermore, for very dim signals, increasing the pinhole size may help due to a higher signal-to-noise ratio and the capture of more photons, aiding in data interpretation.

For super-resolution imaging, particular attention should be taken for deconvolution processing to avoid generating under- or over-processed images that are poorly resolved, as illustrated in Figure 3. Finally, to achieve an optimal 3D reconstruction, setting the best interval determined by the software is strongly recommended. An interval too large between z-sections (i.e., higher than 0.5 μm) will lead to poor 3D rendering and will affect the subsequent analysis of the phenotype.

Advantage of super-resolution over traditional confocal microscopy when imaging BM intracellular trafficking

As illustrated in the results section, although the localization and distribution of BM proteins can be accurately assessed using confocal imaging, the super-resolution approach described generates more precise imaging data with a significant increase in the resolution of intracellular structures containing BM proteins, as well as an enhanced signal-to-noise ratio. Moreover, this super-resolution microscopy technique is relatively easy to use. Since super-resolution imaging significantly increases resolution compared to confocal microscopy, up to 120 nm in the x- and y-axes and 350 nm in z-axis, this approach will greatly impact our understanding of the polarized deposition of BM by more accurately characterizing the intracellular trafficking and secretion of BM proteins in epithelial cells such as the FCs.

Moreover, another super-resolution imaging approach (Structured Illumination Microscopy, SIM) and the use of deconvolution algorithms designed for point-scanning confocal microscopy (i.e., Nikon's enhanced resolution software module) have been used previously to characterize the role of factors involved in BM deposition[29]. The increased resolution associated with these techniques have provided key insight into our understanding of the intracellular trafficking of BM proteins and the organization of the BM. However, these approaches present some limitations compared to Airyscan microscopy. For instance, SIM is not very efficient at acquiring optimal images when obtaining optical z-sections deep in the tissue. This makes SIM difficult to use when screening for new components involved in BM deposition. In addition, the use of deconvolution algorithms applied to confocal images does not achieve the same level of super-resolution. Overall, Airyscan super-resolution imaging on fixed tissue is a powerful and superior approach to study BM intracellular trafficking and deposition.

However, as with any other super-resolution microscopy, a few inconveniences are also associated with this approach, and need to be taken into account while imaging. First, the super-resolution mode usually requires longer acquisition time of the sample than confocal mode. Thus, the acquisition parameters and the region of interest have to be set carefully to minimize photobleaching the sample. Moreover, image files generated by super-resolution microscopy are much larger than files generated by confocal microscopy and may need specialized computers or servers for image processing and storage.

Finally, live imaging of the BM proteins during *Drosophila* oogenesis has been used to characterize new factors involved in BM polarity[57]. However, this approach has limitations, specifically in the resolution of intracellular structures during BM protein trafficking. Super-resolution microscopy is a powerful approach to use in conjunction with live imaging to precisely determine the roles of identified factors in the polarized deposition of BM proteins.

Other applications of this method to study the localization of intracellular components dedicated to vesicular trafficking using endogenously tagged proteins and super-resolution imaging

The establishment and maintenance of tissues and organs during development and in an adult organism rely in part on cell-to-cell signaling and cellular tension and adhesion. These processes depend on intracellular trafficking, endocytosis, exocytosis, and secretion of specific proteins. Thus, the methods described herein to decipher the intracellular trafficking of BM using endogenously tagged proteins and confocal and super-resolution microscopy could be easily adapted to study each process. Moreover, the ease of use of CRISPR/Cas9-mediated genetic editing to generate endogenously tagged proteins make this approach even more versatile and powerful[58].

In conclusion, we have described methods for the preparation and imaging of BM proteins in the FE of the *Drosophila* ovary using confocal and super-resolution microscopy. These protocols can be applied for high-throughput screening to identify new components dedicated to the proper placement of BM proteins. Finally, the employment of this methodology has the potential to make significant contributions to our understanding of

how epithelial cells control the polarized secretion of BM proteins, a key process in the establishment and maintenance of epithelial architecture.

Acknowledgments

The authors are grateful to Julie Merkle for her helpful comments on the manuscript. This work was supported by NIH grant R15GM137236 to O.D. The confocal and super-resolution images were acquired using a Zeiss LSM 900 with Airyscan 2, purchased with NSF MRI grant 2018748.

References

1. Halfter W et al. New concepts in basement membrane biology. FEBS Journal. 282 (23), 4466–4479 (2015). [PubMed: 26299746]
2. Sekiguchi R, Yamada KM Basement membranes in development and disease. Current Topics in Developmental Biology. 130, 143–191 (2018). [PubMed: 29853176]
3. Jayadev R, Sherwood DR Basement membranes. Current Biology. 27 (6), R207–R211 (2017). [PubMed: 28324731]
4. Engelhardt B, Vajkoczy P, Weller RO The movers and shapers in immune privilege of the CNS. Nature Immunology. 18 (2), 123–131 (2017). [PubMed: 28092374]
5. Kefalides N, Borel J Functions of basement membranes. Current Topics in Membranes. 56, 79–111 (2005).
6. Kefalides N, Borel J Basement membranes in development. Current Topics in Membranes. 56, 43–77 (2005).
7. Halfter W et al. The bi-functional organization of human basement membranes. PLoS One. 8 (7), e67660 (2013). [PubMed: 23844050]
8. Morrissey MA, Sherwood DR An active role for basement membrane assembly and modification in tissue sculpting. Journal of Cell Science. 128 (9), 1661–1668 (2015). [PubMed: 25717004]
9. Miller RT Mechanical properties of basement membrane in health and disease. Matrix Biology. 57–58, 366–373 (2017).
10. Mak KM, Mei R Basement membrane type IV collagen and laminin: An overview of their biology and value as fibrosis biomarkers of liver disease. Anatomical Record. 300 (8), 1371–1390 (2017).
11. Fukumoto S et al. Laminin α5 is required for dental epithelium growth and polarity and the development of tooth bud and shape. Journal of Biological Chemistry. 281 (8), 5008–5016 (2006). [PubMed: 16365040]
12. Plachot C et al. Factors necessary to produce basoapical polarity in human glandular epithelium formed in conventional and high-throughput three-dimensional culture: Example of the breast epithelium. BMC Biology. 7, 77 (2009). [PubMed: 19917093]
13. Bonnans C, Chou J, Werb Z Remodelling the extracellular matrix in development and disease. Nature Reviews Molecular Cell Biology. 15 (12), 786–801 (2014). [PubMed: 25415508]
14. Loscertales M et al. Type IV collagen drives alveolar epithelial-endothelial association and the morphogenetic movements of septation. BMC Biology. 14, 59 (2016). [PubMed: 27412481]
15. Kalluri R Basement membranes: Structure, assembly and role in tumour angiogenesis. Nature Reviews Cancer. 3 (6), 422–433 (2003). [PubMed: 12778132]
16. Royer C, Lu X Epithelial cell polarity: A major gatekeeper against cancer. Cell Death and Differentiation. 18 (9), 1470–1477 (2011). [PubMed: 21617693]
17. McLaughlin JM, Bratu DP Drosophila melanogaster oogenesis: An overview. Methods in Molecular Biology (Clifton, N.J.). 1328, 1–20 (2015).
18. Wu X, Tanwar PS, Raftery LA Drosophila follicle cells: morphogenesis in an eggshell. Seminars in Cell & Developmental Biology. 19 (3), 271–282 (2008). [PubMed: 18304845]
19. Horne-Badovinac S, Bilder D Mass transit: Epithelial morphogenesis in the Drosophila egg chamber. Developmental Dynamics: An Official Publication of the American Association of Anatomists. 232 (3), 559–574 (2005). [PubMed: 15704134]

20. Lerner DW et al. A Rab10-dependent mechanism for polarized basement membrane secretion during organ morphogenesis. Developmental Cell. 24 (2), 159–168 (2013). [PubMed: 23369713]
21. Schneider M et al. Perlecan and Dystroglycan act at the basal side of the Drosophila follicular epithelium to maintain epithelial organization. Development (Cambridge, England). 133 (19), 3805–3815 (2006). [PubMed: 16943280]
22. Mao M, Alavi MV, Labelle-Dumais C, Gould DB Type IV collagens and basement membrane diseases: Cell biology and pathogenic mechanisms. Current Topics in Membranes. 76, 61–116 (2015). [PubMed: 26610912]
23. Myllylä R et al. Expanding the lysyl hydroxylase toolbox: new insights into the localization and activities of lysyl hydroxylase 3 (LH3). Journal of Cellular Physiology. 212 (2), 323–329 (2007). [PubMed: 17516569]
24. Myllyharju J, Kivirikko KI Collagens, modifying enzymes and their mutations in humans, flies and worms. Trends in Genetics: TIG. 20 (1), 33–43 (2004). [PubMed: 14698617]
25. Norman KR, Moerman DG The let-268 locus of Caenorhabditis elegans encodes a procollagen lysyl hydroxylase that is essential for type IV collagen secretion. Developmental Biology. 227 (2), 690–705 (2000). [PubMed: 11071784]
26. Rautavuoma K et al. Premature aggregation of type IV collagen and early lethality in lysyl hydroxylase 3 null mice. Proceedings of the National Academy of Sciences of the United States of America. 101 (39), 14120–14125 (2004). [PubMed: 15377789]
27. Saito K et al. TANGO1 facilitates cargo loading at endoplasmic reticulum exit sites. Cell. 136 (5), 891–902 (2009). [PubMed: 19269366]
28. Denef N et al. Crag regulates epithelial architecture and polarized deposition of basement membrane proteins in Drosophila. Developmental Cell. 14 (3), 354–364 (2008). [PubMed: 18331716]
29. Devergne O, Sun GH, Schüpbach T Stratum, a homolog of the human GEF Mss4, partnered with Rab8, controls the basal restriction of basement membrane proteins in epithelial cells. Cell Reports. 18 (8), 1831–1839 (2017). [PubMed: 28228250]
30. Devergne O, Tsung K, Barcelo G, Schüpbach T Polarized deposition of basement membrane proteins depends on Phosphatidylinositol synthase and the levels of Phosphatidylinositol 4,5-bisphosphate. Proceedings of the National Academy of Sciences of the United States of America. 111 (21), 7689–7694 (2014). [PubMed: 24828534]
31. Zajac AL, Horne-Badovinac S Kinesin-directed secretion of basement membrane proteins to a subdomain of the basolateral surface in Drosophila epithelial cells. Current Biology: CB. 32 (4), 735–748.e10 (2022). [PubMed: 35021047]
32. Morin X, Daneman R, Zavortink M, Chia W A protein trap strategy to detect GFP-tagged proteins expressed from their endogenous loci in Drosophila. Proceedings of the National Academy of Sciences of the United States of America. 98 (26), 15050 (2001). [PubMed: 11742088]
33. Buszczak M et al. The carnegie protein trap library: a versatile tool for Drosophila developmental studies. Genetics. 175 (3), 1505–1531 (2007). [PubMed: 17194782]
34. Hales KG, Korey CA, Larracuente AM, Roberts DM Genetics on the fly: A primer on the drosophila model system. Genetics. 201 (3), 815–842 (2015). [PubMed: 26564900]
35. Dunst S, Tomancak P Imaging flies by fluorescence microscopy: Principles, technologies, and applications. Genetics. 211 (1), 15–34 (2019). [PubMed: 30626639]
36. Elliott AD Confocal Microscopy: Principles and Modern Practices. Current Protocols in Cytometry. 92 (1), e68 (2020). [PubMed: 31876974]
37. Sanderson MJ, Smith I, Parker I, Bootman MD Fluorescence microscopy. Cold Spring Harbor Protocols. 2014 (10), pdb.top071795 (2014). [PubMed: 25275114]
38. Liu S, Huh H, Lee SH, Huang F Three-dimensional single-molecule localization microscopy in whole-cell and tissue specimens. Annual Review of Biomedical Engineering. 22, 155–184 (2020).
39. Rust MJ, Bates M, Zhuang X Sub-diffraction-limit imaging by stochastic optical reconstruction microscopy (STORM). Nature Methods. 3 (10), 793–795 (2006). [PubMed: 16896339]
40. Huang B, Babcock H, Zhuang X Breaking the diffraction barrier: Super-resolution imaging of cells. Cell. 143 (7), 1047–1058 (2010). [PubMed: 21168201]

41. Betzig E et al. Imaging intracellular fluorescent proteins at nanometer resolution. Science (New York, N.Y.). 313 (5793), 1642–1645 (2006). [PubMed: 16902090]
42. Heintzmann R, Huser T Super-resolution structured illumination microscopy. Chemical Reviews. 117 (23), 13890–13908 (2017). [PubMed: 29125755]
43. Müller T, Schumann C, Kraegeloh A STED microscopy and its applications: new insights into cellular processes on the nanoscale. Chemphyschem: A European Journal of Chemical Physics and Physical Chemistry. 13 (8), 1986–2000 (2012). [PubMed: 22374829]
44. Feng H, Wang X, Xu Z, Zhang X, Gao Y Super-resolution fluorescence microscopy for single cell imaging. Advances in Experimental Medicine and Biology. 1068, 59–71 (2018). [PubMed: 29943296]
45. Huff J The Airyscan detector from ZEISS: confocal imaging with improved signal-to-noise ratio and super-resolution. Nature Methods. 12, i–ii (2015).
46. Wu X, Hammer JA ZEISS Airyscan: Optimizing usage for fast, gentle, super-resolution imaging. Methods in Molecular Biology (Clifton, N.J.). 2304, 111–130 (2021).
47. Sivaguru M et al. Comparative performance of airyscan and structured illumination superresolution microscopy in the study of the surface texture and 3D shape of pollen. Microscopy Research and Technique. 81 (2), 101–114 (2018). [PubMed: 27476493]
48. Tröger J et al. Comparison of multiscale imaging methods for brain research. Cells. 9 (6), 1377 (2020). [PubMed: 32492970]
49. Zhang W et al. Virtual single-pixel imaging-based deconvolution method for spatial resolution improvement in wide-field fluorescence microscopy. Biomedical Optics Express. 11 (7), 3648 (2020). [PubMed: 33014557]
50. He T, Sun Y, Qi J, Hu J, Huang H Image deconvolution for confocal laser scanning microscopy using constrained total variation with a gradient field. Applied Optics. 58 (14), 3754 (2019). [PubMed: 31158185]
51. Korobchevskaya K, Lagerholm BC, Colin-York H, Fritzsche M Exploring the Potential of Airyscan Microscopy for Live Cell Imaging. Photonics. 4 (3), 41 (2017).
52. Pulver SR, Berni J The fundamentals of flying: Simple and inexpensive strategies for employing drosophila genetics in neuroscience teaching laboratories. Journal of Undergraduate Neuroscience Education: JUNE: A Publication of FUN, Faculty for Undergraduate Neuroscience. 11 (1), A139–A148 (2012). [PubMed: 23493248]
53. Wong LC, Schedl P Dissection of drosophila ovaries. Journal of Visualized Experiments: JoVE. (1), 52 (2006). [PubMed: 18704176]
54. Hudson AM, Cooley L Methods for studying oogenesis. Methods. 68 (1), 207–217 (2014). [PubMed: 24440745]
55. Thompson L, Randolph K, Norvell A Basic techniques in drosophila ovary preparation. Methods in Molecular Biology (Clifton, N.J.). 1328, 21–28 (2015).
56. Long DE et al. A guide for using NIH Image J for single slice cross-sectional area and composition analysis of the thigh from computed tomography. PLoS One. 14 (2), e0211629 (2019). [PubMed: 30730923]
57. Cetera M, Lewellyn L, Horne-Badovinac S Cultivation and live imaging of drosophila ovaries. Methods in Molecular Biology (Clifton, N.J.). 1478, 215–226 (2016).
58. Bier E et al. Advances in engineering the fly genome with the CRISPR-Cas system. Genetics. 208 (1), 1–18 (2018). [PubMed: 29301946]

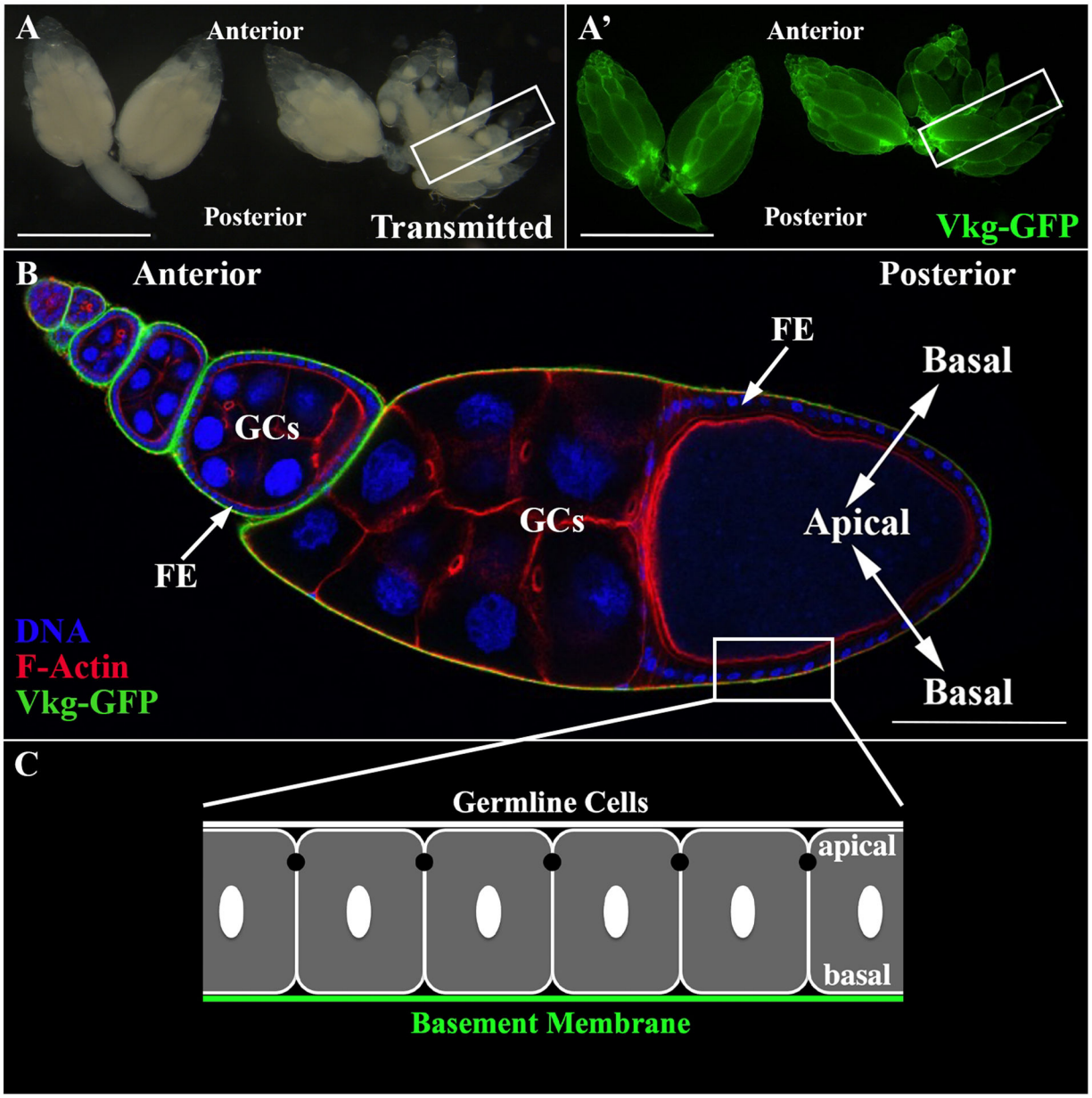

Figure 1: The follicular epithelium (FE) of the *Drosophila* ovary: a model system to study the polarized deposition of basement membrane (BM) proteins.

(**A**) Image of intact ovaries after dissection and excision taken with a fluorescence stereomicroscope. Ovaries are expressing an endogenous GFP-tagged BM protein (Vkg-GFP). Scale bar = 1 mm. (**A'**) Two ovaries of a female fly are attached at the oviduct. Each ovary contains 16–20 ovarioles. A single ovariole is outlined (rectangle). Scale bar = 1 mm. (**B**) Longitudinal section, taken with a confocal microscope, through an ovariole expressing Vkg-GFP and stained for DNA (blue) and F-Actin (red). Ovarioles consist of egg chambers at different stages. Egg chambers are composed of a monolayer follicular epithelium (FE) that surrounds the germline cells (GCs). The FE synthesizes and basally secretes BM proteins (e.g., Pcan and Vkg). Scale bar = 100 μm. (**C**) Schematic of the FE.

The FE is a classic epithelium with a distinct apical-basal polarity where the apical domain faces the germline cells, and the basal domain faces the BM (green).

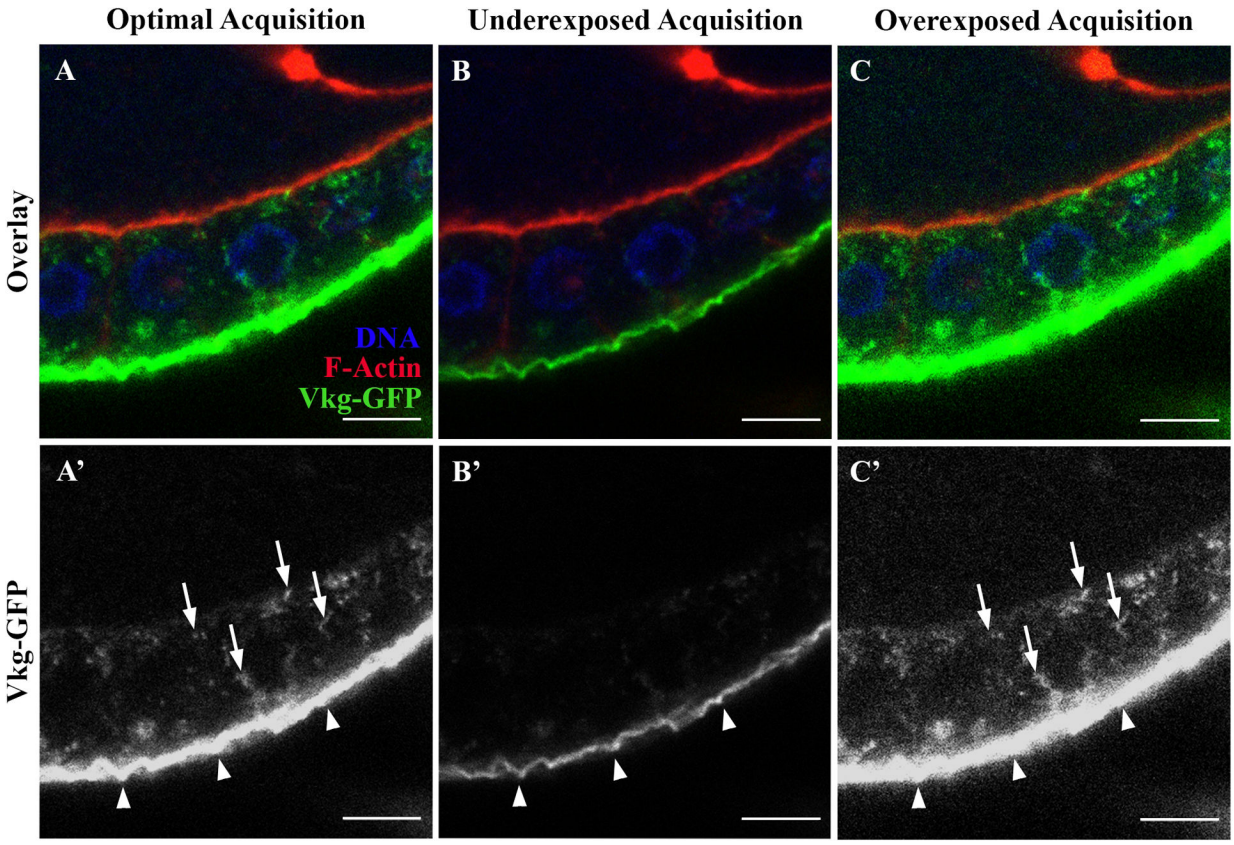

Figure 2: Imaging the intracellular trafficking of BM proteins using confocal imaging.

(**A-C**) Longitudinal section through an egg chamber expressing Vkg-GFP (green) and stained for DNA (blue) and F-Actin (red). (**A'-C'**) Intracellular compartments and vesicles containing Vkg-GFP (arrows), and the basally and extracellularly deposited BM (arrowheads) are shown using confocal microscopy. (**A**) Optimally acquired image for which the intracellular trafficking of Vkg-GFP is visible. (**A'**) Vkg-GFP is localized throughout the cytoplasm of FCs in different cellular compartments (e.g., Golgi) and in vesicles. Due to the fibril organization of Collagen IV, Vkg-GFP-containing vesicles appear elongated (arrows). (**B**) Underexposed image for which the acquisition parameters are optimized to visualize the extracellular BM and not the intracellular distribution of BM proteins. Vkg-GFP (green) appears dim throughout the cytoplasm (**B'**), resulting in undetectable Vkg-GFP-containing vesicles compared to (**A**). (**C**) Overexposed image for which the GFP detector is saturated, resulting in an increase of background fluorescence. Although the intracellular distribution of Vkg-GFP (green) can be seen localized throughout the cytoplasm of the FCs (arrows), overexposure results in imaging artifacts where the intracellular structures appear larger than they are, as in (**A-A'**). Scale bars = 5 μm.

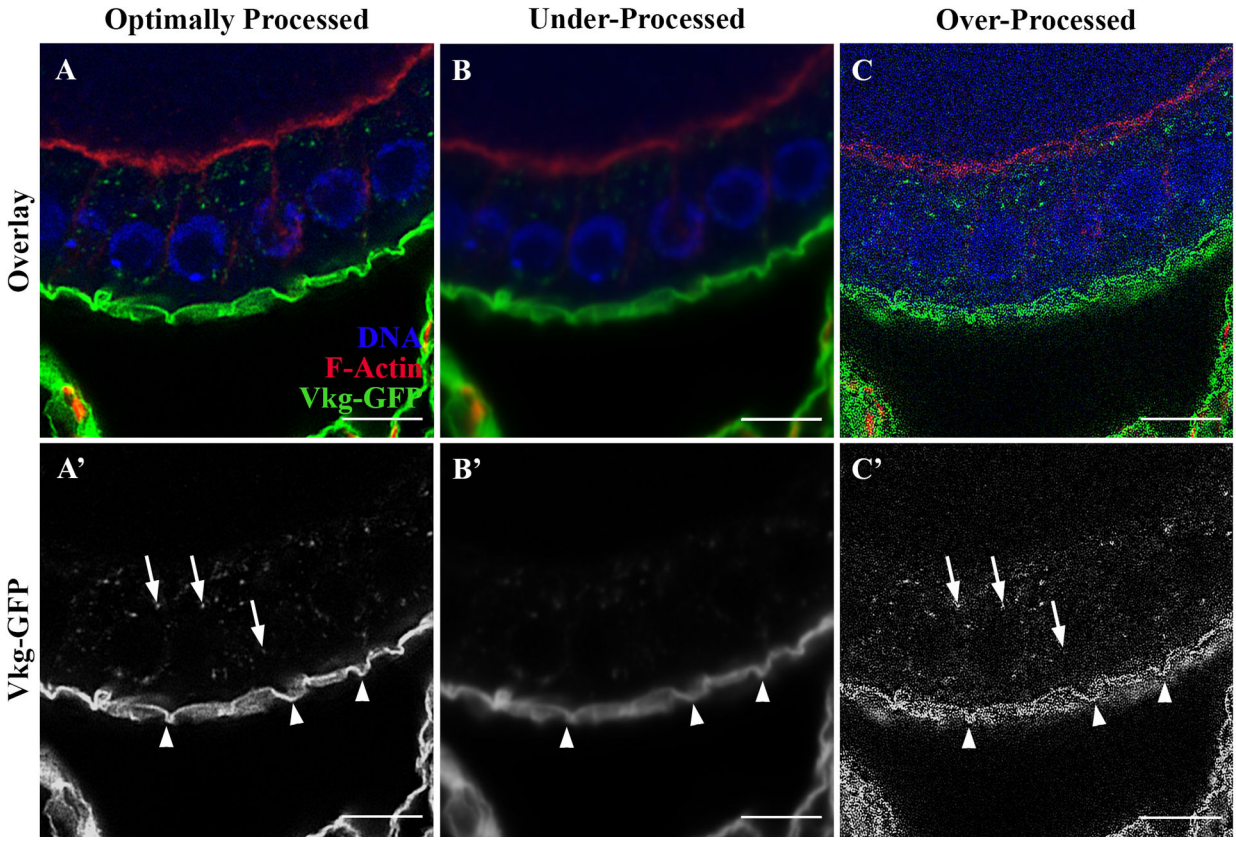

Figure 3: Imaging the intracellular trafficking of BM proteins using super-resolution imaging and processing.

(**A-C**) Longitudinal section through an egg chamber expressing Vkg-GFP (green) and stained for DNA (blue) and F-Actin (red). (**A**) Optimally processed super-resolution image, in which the intracellular trafficking of Vkg-GFP is clearly observed. (**A'**) Vkg-GFP is localized throughout the cytoplasm of the FCs in different cellular compartments (e.g., Golgi) and vesicles (arrows) and at the BM (arrowheads). (**B**) Under-processed image resulting in higher background fluorescence than in (A). The intracellular localization of Vkg-GFP (green) appears dim and less defined (compare B with A). (**C**) Over-processed image resulting in an image where the intracellular localization of Vkg-GFP appears pixelated and grainy. Scale bars = 5 μm.

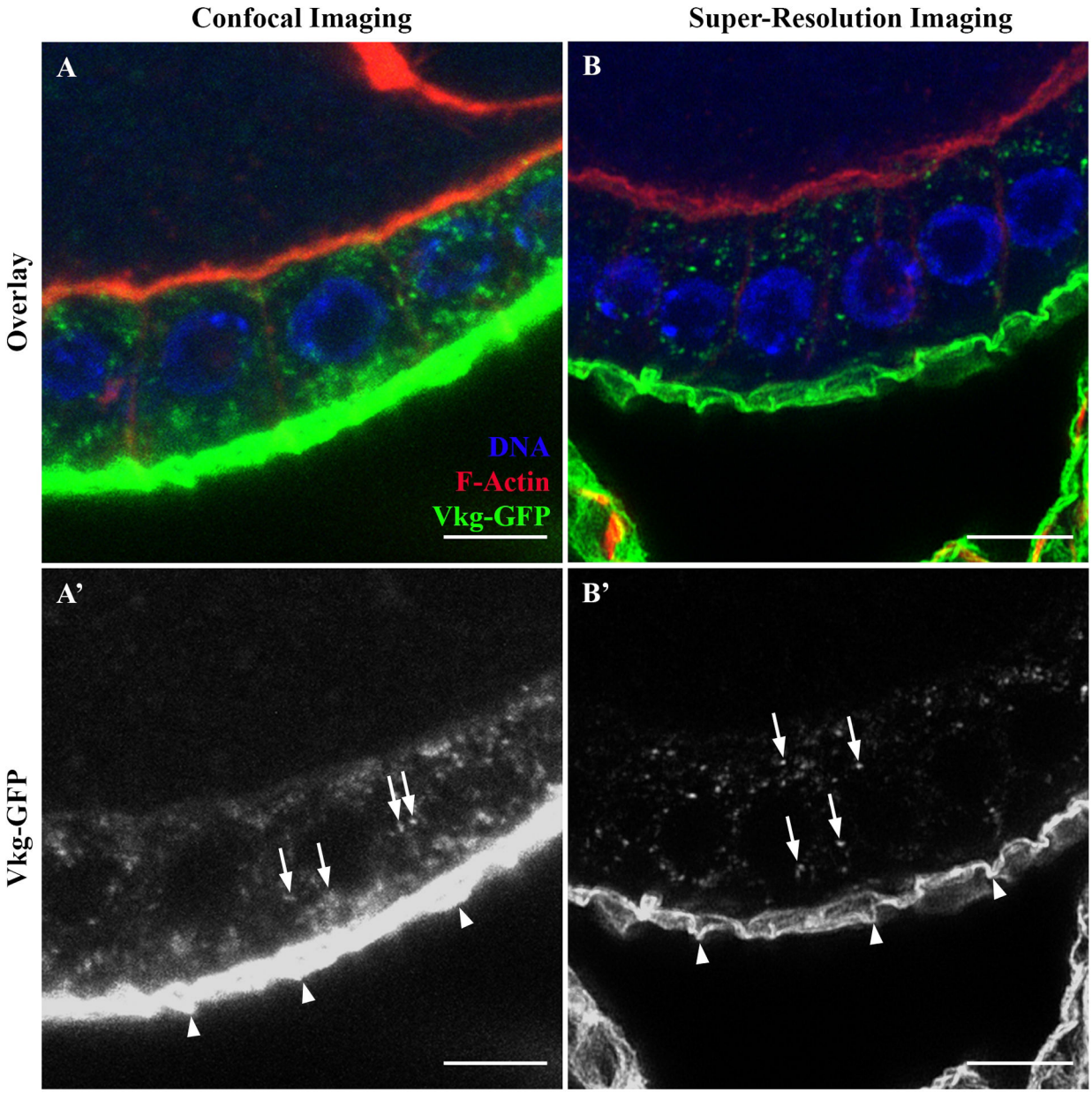

Figure 4: Orthogonal projection of a z-stack acquired and processed using confocal and super-resolution microscopy approaches.

(**A**-**B**) Orthogonal projection of optical z-sections through an egg chamber expressing Vkg-GFP (green) and stained for DNA (blue) and F-Actin (red) using confocal (**A**) or super-resolution (**B**) microscopy. (**A**) Projection of a z-stack acquired using optimal confocal parameters. The intracellular localization of Vkg-GFP can be observed throughout the z-axis in the FCs (**A'**, arrows). The BM is also visible and appears very bright (**A'**, arrowheads). (**B**) Projection of a z-stack acquired using optimal super-resolution processing. Well-defined intracellular compartments and vesicles containing Vkg-GFP can be observed throughout the z-axis in the FCs (**B'**, arrows). The BM is also very well-defined (**B'**, arrowheads). The difference between standard confocal imaging and super-resolution imaging is apparent, as the intracellular localization of Vkg-GFP and the BM are significantly more defined when

using super-resolution than standard confocal microscopy. Moreover, the image taken by confocal microscopy has higher background fluorescence. Scale bars = 5 μm.

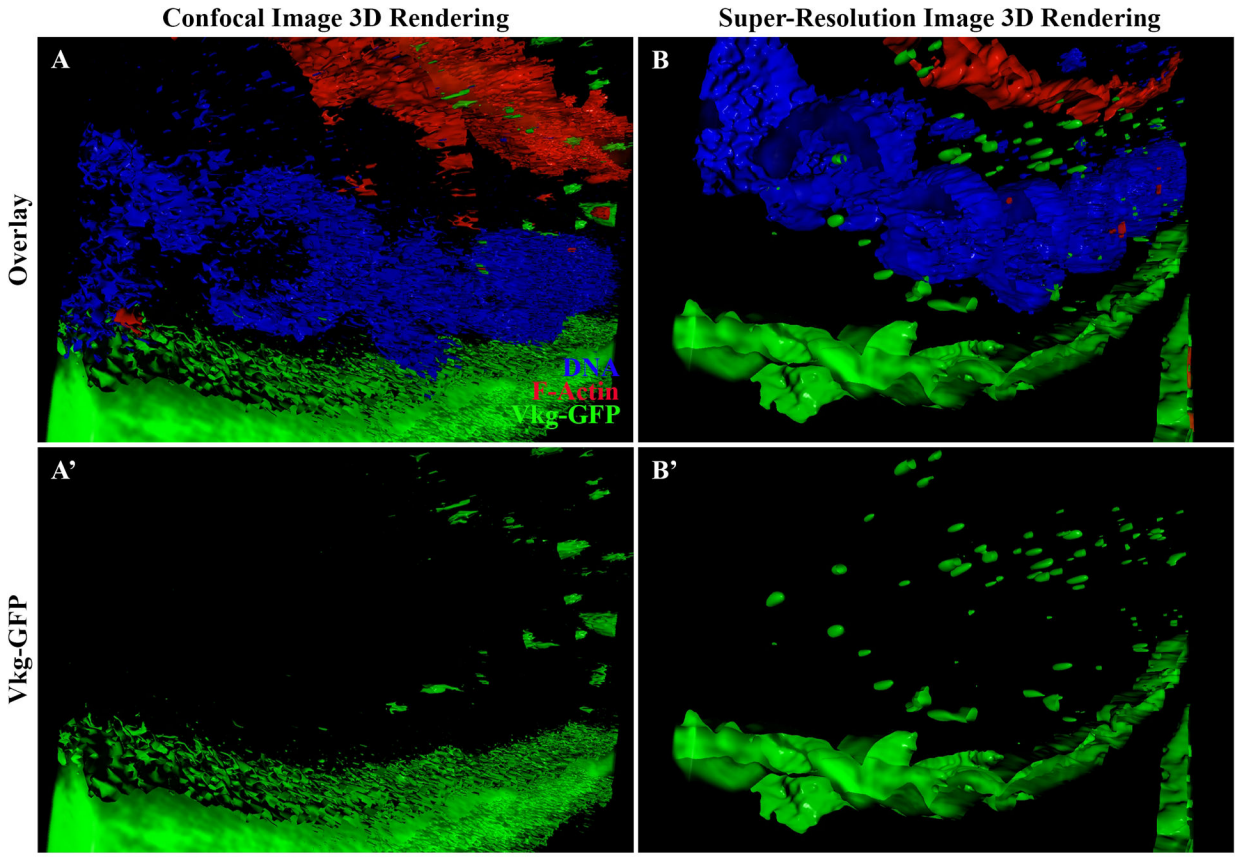

Figure 5: 3D reconstruction of a z-stack acquired and processed using confocal and super-resolution microscopy approaches.

(**A-B**) 3D rendering of z-stacks (mixed view) of egg chambers expressing Vkg-GFP (green) and stained for DNA (blue) and F-actin (red). (**A**) 3D rendering of a z-stack acquired *via* confocal microscopy. The location and shape of compartments and vesicles containing Vkg-GFP can be seen throughout the cells (**A'**). (**B**) 3D rendering of a z-stack acquired *via* optimal super-resolution processing. The location and shape of compartments and vesicles containing Vkg-GFP can be seen (**B'**). The shape of vesicles, as well as the BM and the nuclei, are smoothly defined, and the resolution is higher compared to that of confocal microscopy (compared B' and A'). The shape and size of the compartments and vesicles containing Vkg-GFP can also be better determined using super-resolution microscopy (compared B' and A').

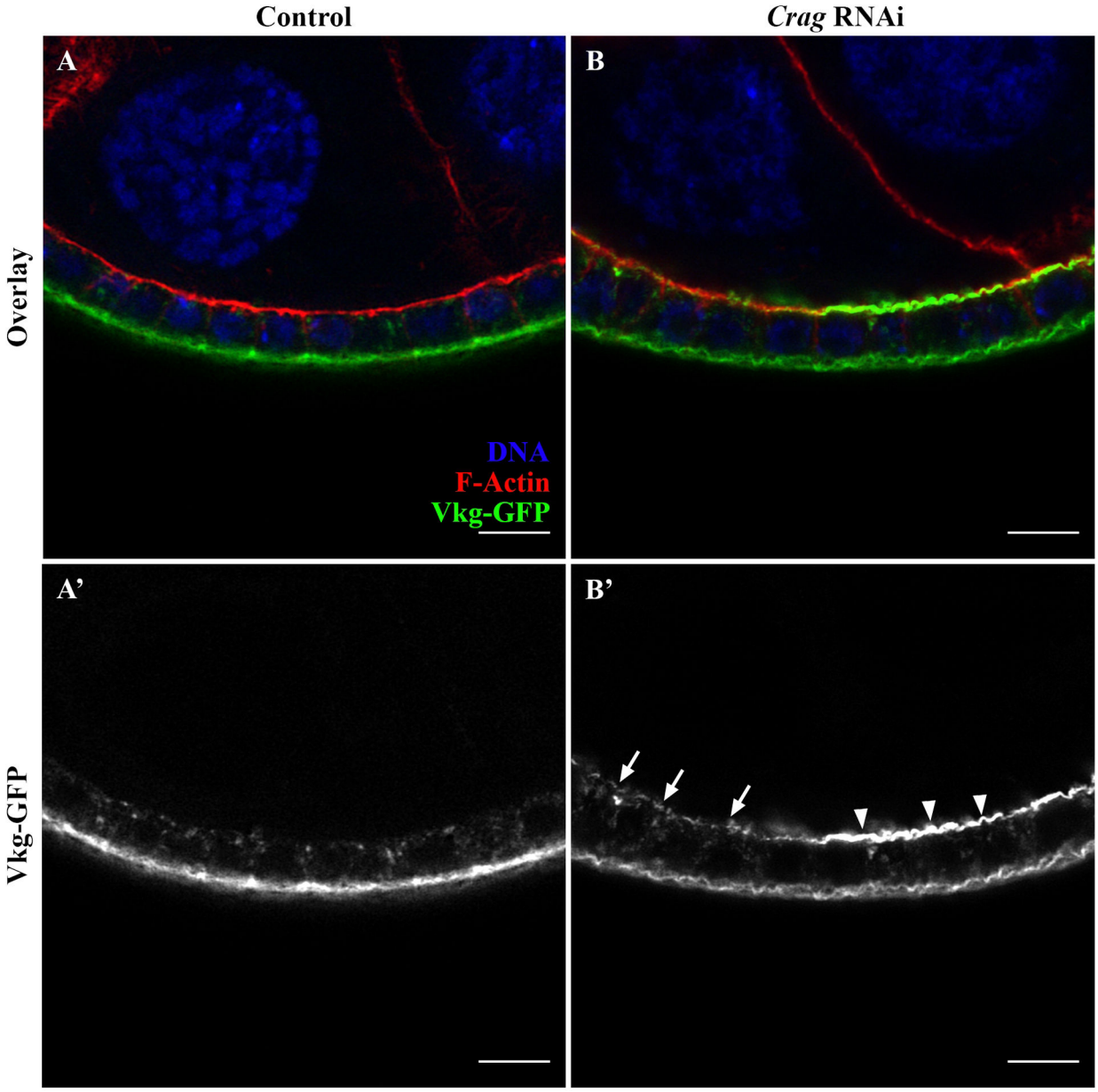

Figure 6: Characterization of Vkg-GFP localization in *Crag* knocked down FCs.

(**A-B**) Longitudinal section through an egg chamber expressing Vkg-GFP (green), stained for DNA (blue) and F-Actin (red) and acquired *via* optimal super-resolution processing. (**A**) Control line expressing wildtype Crag, a protein critical for proper BM deposition. The FE shows typical BM protein localization, wherein Vkg-GFP is intracellularly distributed and deposited basally in the FE (**A'**). (**B**) Transgenic *Drosophila* line expressing RNAi for *Crag* in the FE, resulting in a *Crag* knockdown. The loss of *Crag* leads to the mislocalization of BM proteins (e.g., Vkg-GFP) apically in the FE (**B'**, arrows and arrowheads). Super-resolution image is used to characterize the BM mislocalization phenotypes associated with the loss of *Crag*. Specifically, some *Crag* RNAi FCs, show a strong apical mislocalization of BM proteins (**B'**, arrowheads), while other *Crag* RNAi FCs present a weaker apical

mislocalization (**B'**, arrows). Super-resolution imaging clearly reveals the phenotypes associated with the loss of *Crag* (**B'**, arrowheads vs arrows). Scale bars = 5 μm.

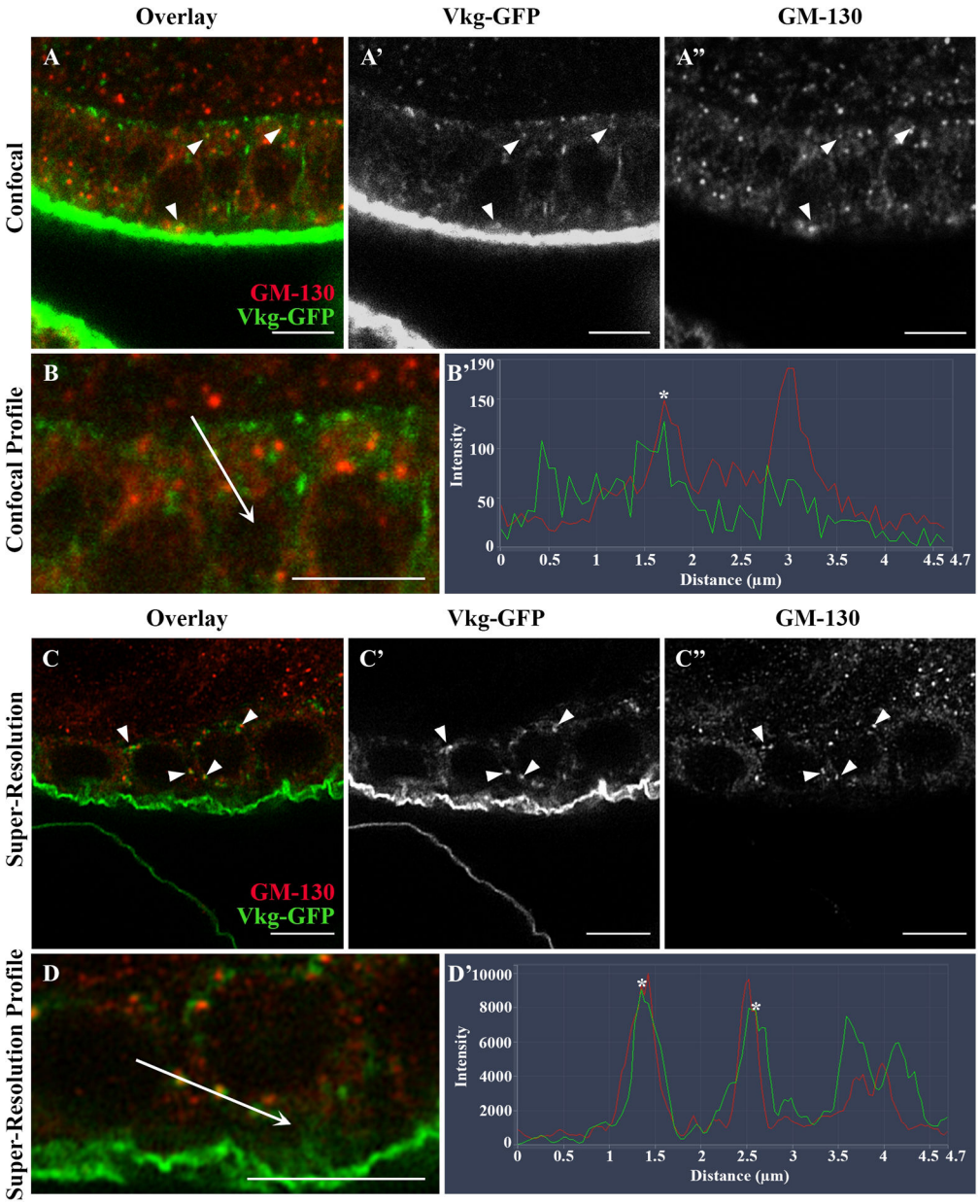

Figure 7: Colocalization of Vkg-GFP and GM-130 (Golgi marker) using confocal and super-resolution microscopy approaches.

(**A-D**) Longitudinal sections through egg chambers expressing Vkg-GFP and immunostained for a cis-Golgi marker (GM-130, red), imaged using confocal (**A,B**) or super-resolution (**C,D**) microscopy. (**A,B**) Confocal imaging shows that intracellular Vkg-GFP partially colocalizes with a cis-Golgi marker (**A**, arrowhead). (**B**) Zoomed-in area of (**A**). The distributions of green (Vkg-GFP) and red (GM-130) pixels along the white arrow are plotted in a histogram (**B'**). The x-axis of the histogram represents the distance (µm) along the arrow while the y-axis represents pixel intensity. The overlapping green and red peaks (*) show where Vkg-GFP and GM-130 colocalize. (**C,D**) Super-resolution imaging also shows that intracellular Vkg-GFP partially colocalizes with a cis-Golgi marker (**C**,

arrowhead). (**D**) Zoomed-in area of (**C**). The distributions of green (Vkg-GFP) and red (GM-130) pixels along the white arrow are plotted in a histogram (**D'**). The x-axis of the histogram represents the distance (μm) along the arrow while the y-axis represents pixel intensity. The overlapping green and red peaks (*) show where Vkg-GFP and GM-130 colocalize. These data show that super-resolution imaging is a more efficient and precise approach than confocal imaging to characterize and quantify colocalization. Scale bars = 5 μm.

Table 1:

Confocal and super-resolution microscopy acquisition and processing parameters for the representative images.

All of the main imaging parameters are compiled for the representative images provided.

Image Acquisition Parameters										
Figure Number			1C	2A	3A	4A	4B	5A	5B	6A	6B
Acquisition Mode			Confocal	Confocal	Airyscan	Confocal	Airyscan	Confocal	Airyscan	Airyscan	Airysca
Objective			Plan-Apochromat 20x/0.8 M27	Plan-Apochromat 63x/1.4 Oil DIC M27	Plan-Apochromat 63x/1.4 Oil DIC M27	Plan-Apochromat 63x/1.4 Oil DIC M27	Plan-Apochromat 63x/1.4 Oil DIC M27	Plan-Apochromat 63x/1.4 Oil DIC M27	Plan-Apochromat 63x/1.4 Oil DIC M27	Plan-Apochromat 63x/1.4 Oil DIC M27	Plan-Apochron 63x/1.4 O DIC M2
Scan Mode			Frame	Frame	Frame	Frame	Frame	Frame	Frame	Frame	Frame
Image Size (Pixels)			5172x5172	359x359	694 x 694	359x359	694 x 694	359 x 359	694 x 694	1040 x 1040	1040 x 10
Image Size (Scaled)			638.90 μm x 638.90 μm	25.35 μm x 25.35 μm	24.51 μm x 25.51 μm	25.35 μm x 25.35 μm	24.51 μm x 25.51 μm	25.35 μm x 25.35 μm	24.51 μm x 25.51 μm	36.71μm x 36.71 μm	36.71μm 36.71 μ
Pinhole Size		640	1 au/ 31 μm	NA	NA	NA	NA	NA	NA	5 au/ 281 μm	5 au/ 28 μm
		561	1 au/ 50 μm	1 au/ 50 μm	5 au/ 247 μm	1 au/ 50 μm	5 au/ 247 μm	1 au/ 50 μm	5 au/ 247 μm	5 au/ 247 μm	5 au/ 24 μm
		488	1 au/ 24 μm	1 au/ 44 μm	5 au/ 219 μm	1 au/ 44 μm	5 au/ 219 μm	1 au/ 44 μm	5 au/ 219 μm	5 au/ 219 μm	5 au/ 21 μm
		405	1 au/ 21 μm	1 au/ 38 μm	5.46 au/ 205 μm	1 au/ 38 μm	5.46 au/ 205 μm	1 au/ 38 μm	5.46 au/ 205 μm	5.46 au/ 205 μm	5.46 au/ 2 μm
Scan Zoom			0.5	4	4	4	4	4	4	2.7	2.7
Pixel Time			0.82 μs	1.48 μs	2.94 μs	1.48 μs	2.94 μs	2.95μs	2.94 μs	0.99 μs	0.73 μs
Frame Time			3 min 24 sec	1.78 s	7.12 s	1.78 s	7.12 s	3.57s	7.12 s	5.26s	30.95 s
LSM Scan Speed			5	9	6	9	6	7	6	7	8
Scan Direction			Bidirectional	Bidirectional	Bidirectional	Bidirectional	Bidirectional	Bidirectional	Bidirectional	Bidirectional	Bidirectio
Averaging (Mean Intensity)			2	2	1	2	1	2	1	1	1
Bits per Pixel			8	8	16	8	16	8	16	16	16
Channels	640	Intensity (%)	0.8	NA	NA	NA	NA	NA	NA	0.8	1.6
		Master Gain (V)	700	NA	NA	NA	NA	NA	NA	840	803
	561	Intensity (%)	0.8	0.7	0.8	0.7	0.8	0.8	0.8	0.9	1.4
		Master Gain (V)	800	700	800	700	800	720	800	880	800
	488	Intensity (%)	0.8	0.8	1	0.8	1	0.9	1	0.8	0.6
		Master Gain (V)	810	800	900	800	900	820	900	830	800
	405	Intensity (%)	0.8	0.7	0.9	0.7	0.9	0.8	0.9	0.9	0.6
		Master Gain (V)	810	780	875	780	875	800	875	850	817

Z-Section Parameters	Range	NA	2.28 µm	1.3 µm	1.14 µm	1.3 µm	2.47 µm	1.3 µm	1.43µm	NA
	Interval	NA	0.19 µm	0.13 µm	0.19	0.13 µm	0.190 µm	0.13 µm	0.13µm	NA
	Slices	NA	13	11	(2–7)	(2–11)	14	11	12	1
Airyscan Processing (SR)		NA	NA	7.3	NA	7.3	NA	6.4	7.1	7.1

Materials

Name	Company	Catalog Number	Comments
Alexa Fluor 546 phalloidin	Invitrogen	A22283	F-Actin Stain (1/500 of 66μM)
Alexa Fluor 647 phalloidin	Invitrogen	A22287	F-Actin Stain (1/100 of 66μM))
Anti-GM130 Antibody	abcam	ab30637	For Golgi Stain (colocalization); use as concentration of 7μg/uL
Aqua-Polymount	Polysciences, Inc.	1860620	Mounting Medium
Bakers Yeast (Active Dry Yeast)	Genesee Scientific	62–103	To fatten the overies for dissection
Bovine Serum Albumin (30% solution)	Sigma-Aldrich	A7284	For blocking solution
Depression wells	Electron Microscopy Sciences	7156101	For dissection (glass concavity slide can be used instead)
Dissecting needle	Fisher scientifc	13–820-024	
Drosophila Incubator	Genesee Scientific/ Invictus		
Fly Stock: Perlecan-GFP *Drosophila* line (ZCL1700)			Morin et al., 2001
Fly Stock: UAS-*Crag* RNAi line (TRIP line HMS00241)	Bloomington Drosophila Stock Center	33594	RNAi against Crag
Fly Stock: Viking-GFP Drosophila line (CC00791)			Buszczak et al., 2007
Fly Stock: Vkg-GFP, tj-Gal4			Devergne et al., 2017. Drive the expression of Crag RNAi in the FE
Forceps (Dumont 5)	Fine Science Tools	11251–30	For dissection
Glass Concavity Slide	Electron Microscopy Sciences	7187804	For dissection (depression wells can be used instead)
Goat anti-Rabbit IgG, Alexa Fluor 568	Invitrogen	A11036	Secondary antibody (GM130 antibody) (5 μg/mL)
Hoechst (Hoechst 33342)	Invitrogen	H3570	DNA Stain (1 ug/mL)
Kimwipes	Kimtech	Fisher Scientific: 06–666	Delicate task wipers
Leica Fluorescent Stereo Microscope M165 FC	Leica		For ovary imaging
Microscope Slides	Corning	294875X25	Microscope Slides
Nutating platform rocker	Corning Life Sciences	6720	For ovary fixation and staining
Nutri-Fly BF	Genesee Scientific	66–121	Fly Food
Paraformaldehyde 20% Solution	Electron Microscopy Sciences	Fisher Scientific: 15713	For PFA 4%
Phosphate Buffered Saline Tablets	Fisher scientific	BP2944100	For PBS solution
ProLong Glass Antifade Mountant	Invitrogen	P36980	Mounting Medium
Square Cover Glass	Corning	285022	Cover glass for microscope slides
Triton x-100	Sigma-Aldrich	9036–19-5	For PBST
Zeiss LSM 900 with Airyscan 2	Zeiss		Confocal and super-resolution Microscope
Zeiss Stemi 305 Stereo Microscope	Zeiss		Dissecting microscope
Zeiss Zen Software version 3.3 (Blue Edition)	Zeiss		Image acquisition and processing